IARJSET

ISSN (O) 2393-8021, ISSN (P) 2394-1588

International Advanced Research Journal in Science, Engineering and Technology

Vol. 8, Issue 8, August 2021

DOI: 10.17148/IARJSET.2021.8803

Role of annealing temperature on Structural and Electric Transport properties of Pure ZnO nanoshapes

Anil Kaushik[1], Dr S. K. Chaudhary[2], Dr Ajay Kumar Mann[3]

Research Scholar, Department of Physics, Baba Mastnath University, Asthal Bohar, Rohtak- 124021(Haryana) [1]

HOD, Department of Physics, Baba Mastnath University, Asthal Bohar, Rohtak- 124021(Haryana) [2]

Department of Physics, Pt. N. R. S. College, Rohtak- 124001(Haryana) [3]

Abstract: We used the co-precipitation method to create pure phase Zinc Oxide nanostructures in this study. X-ray diffraction was used to investigate the phase and scale of synthesised nanostructures (XRD). The ZnO sample calcined at 400 °C has a crystalline size of 36.1 nm, an inter planner spacing of 2.7010 Å, and a volume of 71.62 $Å^3$. The morphological research was done using a scanning electron microscope (SEM). The IR peaks near around 510 cm^{-1} correspond to stretching of the Zn-O bonds, according to IR studies conducted with an FTIR spectrometer. A kaithely source metre was used to measure the current-voltage characteristics and resistivity of zinc oxide nanostructures. Impedance spectroscopy of synthesised samples was performed at room temperature using a galvinostat with an applied voltage of 120 mV and a frequency range of 50 Hz to 5 MHz. For ZnO calcined at 400°C, the grain boundary resistance is about 32 MΩ (at 310 K).

Keywords: Zinc Oxide, X-RD, SEM, FTIR, AC Impedance Spectroscopy.

1. INTRODUCTION

The structural, morphological, mechanical, and optical properties of metal oxide semiconductors are excellent. Due to its large band gap semiconductor (E_g=3.21-3.83 eV) and numerous applications in sensor, catalysis, actuators, spintronics, and photovoltaic devices, ZnO has gotten a lot of attention in recent decades [1,2]. Various synthesis methods, such as sol-gel, co-perception, hydrothermal, and thermal evaporation, were used to synthesise ZnO nano structures. Among these techniques, the co-perception approach is most likely to synthesise ZnO nano structures in large enough amounts and at a low cost for industrial applications. Because of its diverse properties, ZnO is one of the most popular metal oxide semiconductors. ZnO is an II–VI semiconductor material with a wide variety of useful properties, making it a very promising material. The ionicity of ZnO lies somewhere between covalent and ionic semiconductor. Wurtzite (B4), zinc blende (B3), and rocksalt are the three types of crystal structures found in ZnO. (B1). However, hexagonal wurtzite is the most stable phase in ambient conditions. The wurtzite structure of Zno is hexagonal (P63mc), with lattice parameters of a = b = 3.239 and c = 5.213 [3]. Zn atoms are tetrahedrally coordinated to four oxygen atoms in ZnO nanostructures, and Zn's 3d electrons hybridise with oxygen's 3p electrons [4]. Numerous pioneers have investigated the photo catalytic and optical properties of ZnO nanoparticles extensively in the literature; however, it is necessary to investigate the effect of annealing on phase, electric, and morphological properties of ZnO nanoparticles. As a result, we present a competent effort to recognise the effect of annealing on phase, electric, and morphological properties of ZnO nanoparticles. As a result, in this study, we used the co-perception method to synthesise ZnO nanostructures and investigated the effect of annealing temperatures on structural, optical, and dielectric properties.

2. EXPERIMENTAL DETAILS:

2.1. Material

Loba (India) uses zinc acetate dehydrate (Zn(CH3COO)2, sodium hydroxide (NaOH), ethanol (C2H5OH), and DI water as starting materials that do not need further purification.

2.2. Synthesis Procedure

The co-precipitation method was used to make ZnO nanoparticles. Initially, the starting materials for the emblematic

IARJSET

ISSN (O) 2393-8021, ISSN (P) 2394-1588

International Advanced Research Journal in Science, Engineering and Technology

Vol. 8, Issue 8, August 2021

DOI: 10.17148/IARJSET.2021.8803

synthesis process were taken in a stoichiometric ratio of zinc acetate dehydrate and sodium hydroxide. The precursors were then dissolved in ethanol and DI water, and the mixture was stirred for 2 hours at 80 degrees Celsius. After that, the solution was left to sit overnight before being washed with DI water and dried in an oven at 90°C for 12 hours. As a result, the powder was annealed for 2 hour at 400 degrees Celsius. After the full combustion process, the white powder was obtained.

2.3. Characterizations

X-ray diffraction (XRD) was used to describe and analyse the crystal phases of synthesised samples. Field Emission Scanning Electron Microscopy measurements were taken for morphological analyses of synthesised samples. The dc resistivity calculation was done with a Keithley 2400 source metre. The AC conductivity tests were carried out at room temperature with an AC impedance analyzer in a frequency range of up to 3MHz.

3. RESULTS AND DISCUSSIONS:

3.1 Structural Analysis:

Figure 1 shows the XRD patterns of synthesised samples of ZnO nanostructures in the range of 2θ (diffraction angle) 20 to 80. The diffraction peaks at 31.71, 34.28, 36.29, 47.57, 56.34, 62.56, 67.93, 69.08, 72.45, 76.96, and 81.52 correspond to hkl (100), (002), (101), (102), (110), (103), (200), and (112), (201) and (202), respectively. The JCPDS card number #80-0075 matched all of the diffraction peaks. The Debye Scherer formula can be used to measure the average crystalline size (D) [2]:

$D = K \lambda / \beta \cos\theta$ ..... (i)

Where k=0.91 is the form factor, 1.54 Å is the wavelength of X-rays with Cu K_α radiation, β is the full width at half maximum (FWHM), θ reflects the instruments broadening, and is the Bragg diffraction angle. Using the Bragg's law relationship, the interplanar spacing (dhkl) was calculated:

$2d\sin\theta = n\lambda$ ..... (ii)

Where ‘n' denotes the diffraction order and θ denotes the diffraction angle.

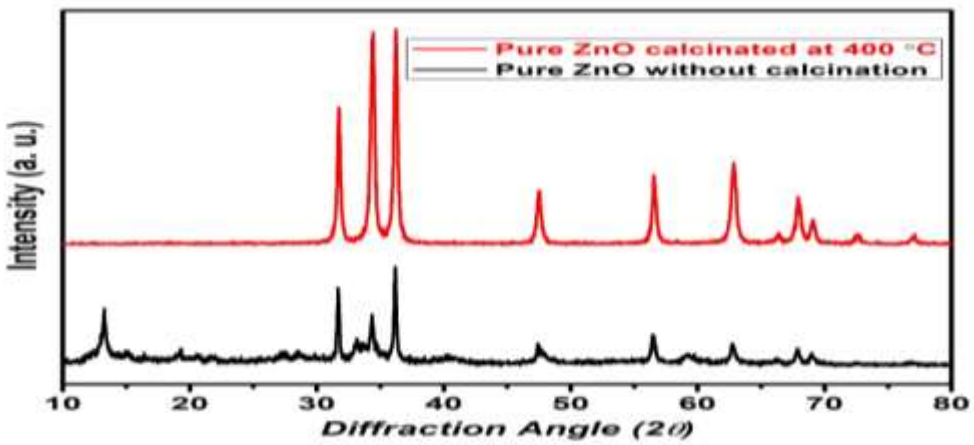

Figure 1. XRD pattern of pure ZnO (without calcinations and calcinated at 400 °C)

The lattice parameters and volume of the synthesized sample's unit cell were calculated using the following equations:

$a = d_{hkl} * \sqrt{h^2 + k^2 + l^2}$ ..... (iii)

$V = 0.88 * a^2 * c$ ..... (iv)

The inter plane spacing is d_{hkl}, the miller indices of the planes are hkl, and the lattice parameters are a and c, which are tabulated in table 1.

IARJSET

ISSN (O) 2393-8021, ISSN (P) 2394-1588

International Advanced Research Journal in Science, Engineering and Technology

Vol. 8, Issue 8, August 2021

DOI: 10.17148/IARJSET.2021.8803

Table 1:

Samples	Crystalline Size (nm)	Inter plane spacing (d_{hkl}) Å	lattice parameters Å		Unit Cell Volume (V) Å^3
			a = b	c	
ZnO calcined at 400˚C	36.1	2.7010	3.7132	5.5861	71.62

3.2 Morphological Analysis:

SEM (Scanning Electron Microscopy) was used to conduct the morphological tests, as shown in Figure 2. As the calcination temperature varied, the morphology of Zinc Oxide samples changed. The agglomerations of nano particles can be seen in the SEM micrograph of ZnO samples.

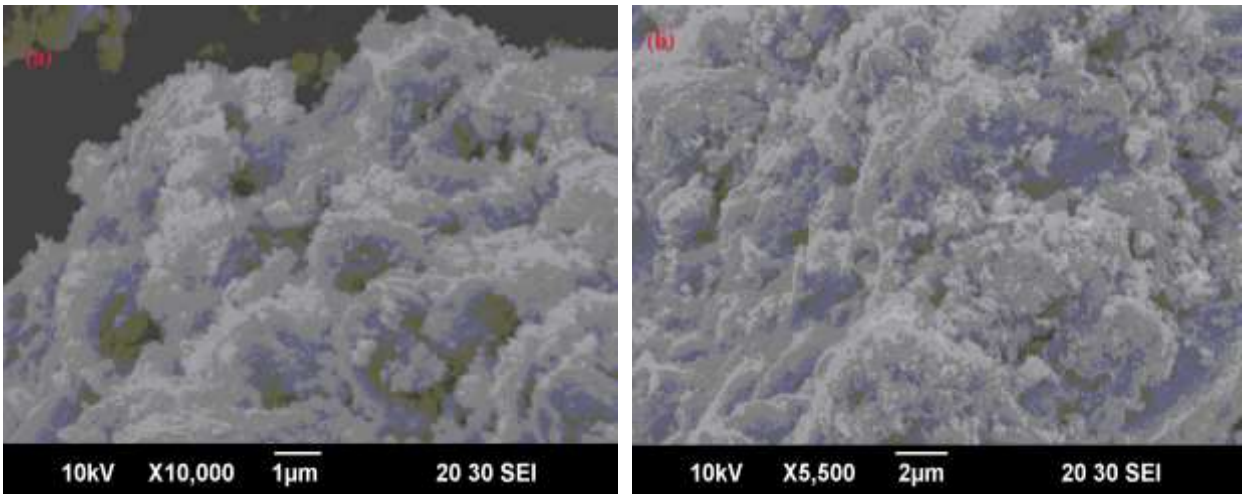

Figure 2 (a-b).: (a) ZnO micrograph without calcinations (b) ZnO micrograph for cacinated at 400 °C

3.3 FT-IR Studies:

Figure 3 shows the FTIR spectrum of ZnO samples in the 500 - 3500 cm^{-1} range. 3365 cm^{-1}, 1554 cm^{-1}, 1376 cm^{-1}, 1042 cm^{-1}, 934 cm^{-1}, 828 cm^{-1}, 669 cm^{-1}, 598 cm^{-1}, and 510 cm^{-1} are the IR peaks in the samples. The vibration of the C-H, C=O, and C-O bonds is represented by the IR peaks in the 710 cm^{-1} to 1690 cm^{-1} range. The peaks around 500 cm^{-1} lead to Zn-O bond stretching [4, 5]. The stretching vibrations of O-H bonds and bending modes of absorbed water, as well as the presence of O=C=O bonds, correspond to the reaming peaks in the area 1690 cm^{-1} – 3365 cm^{-1}.

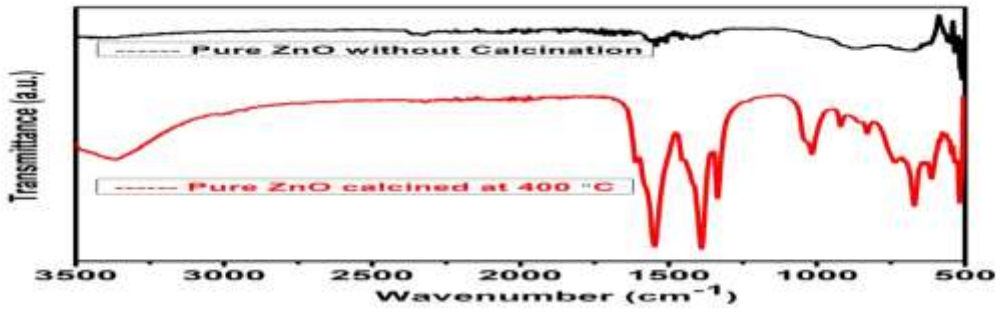

Figure 3. FTIR spectra of ZnO without calcinations and calcinated at 400 °C

IARJSET ISSN (O) 2393-8021, ISSN (P) 2394-1588

International Advanced Research Journal in Science, Engineering and Technology

Vol. 8, Issue 8, August 2021

DOI: 10.17148/IARJSET.2021.8803

The IR peaks sharply appear in the range 510 cm^{-1} to 1545 cm^{-1} as the calcination temperature increases for ZnO sample, which is due to the presence of compressive stress on ZnO nanoparticles, increase in crystalline nature of ZnO, and variation in morphology of ZnO, as shown in XRD spectra and SEM micrograph of 400 °C calcined ZnO sample.

3.4 Complex Impedance Studies:

At room temperature, the electric activity of Zinc Oxide samples was investigated using complex impedance spectroscopy over a broad frequency spectrum. Figure 4 shows the nyquist plots of ZnO (calcined at 400°C). An equation gives the complex impedance (Z):

$Z = Z' - jZ''$ ..... (v)

Where Z is the real part of complex impedance and Z is the imaginary part. The single semicircular curve formation in the cole-cole (Nyquist) plot confirms the presence of grains and a distinct relaxation mechanism in the synthesised ZnO samples.

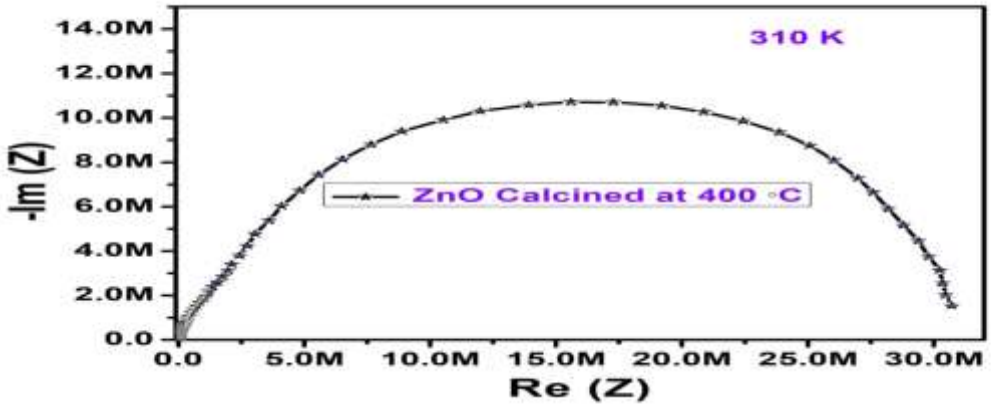

Figure 4. Nyquist plot of pure ZnO calcinated at 400 °C

This spectroscopic technique is used to separate the true and imaginary parts of electronic parameters such as impedance (Z), permittivity (ε), dielectric loss (tanδ), and admittance (Y), among others. Furthermore, figure 5 depicts the variance of the real component (Z) of complex impedance as a function of frequency at room temperature, and it is evident from the graph that the values of Z abruptly decrease as the frequency increases, owing to an increase in AC conductivity due to hopping conduction phenomena [6,7]. As a result, the actual component of impedance has a heavy frequency dependent behaviour in the low frequency range, which leads to higher resistivity and high grain boundary resistance values, while Z has a frequency independent behaviour in the higher frequency range. In addition, figure 6 depicts the variance of Z as a function of frequency, which exhibits a similar pattern to Z. The grain and grain boundary of the crystal system are split using Complex Impedance Spectroscopy (CIS), which corresponds to the low and high frequency dispersion field [8,9].

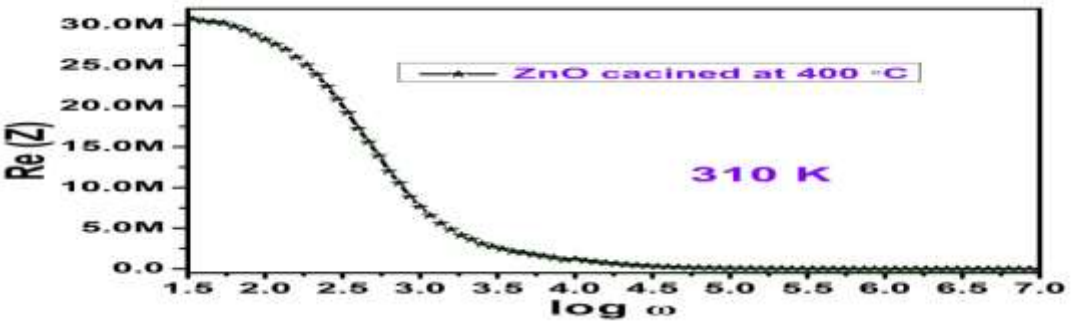

Figure 5: variation of Real part of complex Impedance with frequency for Pure ZnO calcinated at 400 °C

IARJSET

ISSN (O) 2393-8021, ISSN (P) 2394-1588

International Advanced Research Journal in Science, Engineering and Technology

Vol. 8, Issue 8, August 2021

DOI: 10.17148/IARJSET.2021.8803

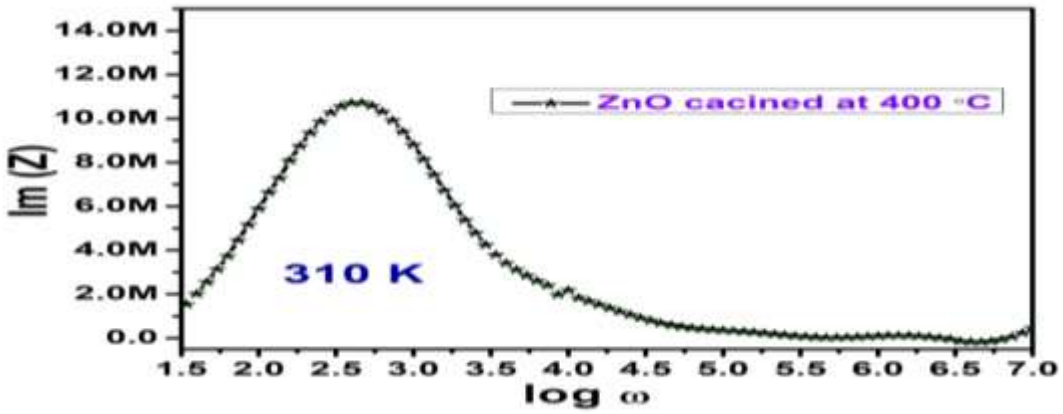

Figure 6: Variation of Imaginary part of complex impedance with frequency for Pure ZnO calcinated at 400 °C

4. CONCLUSION

To investigate the effect of annealing on the synthesis process and properties, the Zinc Oxide (ZnO) samples were successfully synthesised using the co-perception technique at different annealing temperatures. The crystalline form, inter planner spacing, and volume of the ZnO sample calcined at 400 °C are 36.1 nm, 2.7010, and 71.62, respectively. Both ZnO samples have excellent structural, morphological, FTIR, and electronic transport properties. The vibration of the C-H, C=O, and C-O bonds is represented by the FTIR peaks in the 705 cm-1 to 1690 cm^{-1} range. The stretching of the Zn-O bonds is defined by the peaks around 510 cm^{-1}. The grain boundary resistance of ZnO calcined at 400 °C is around 32 MΩ (at 310 K). In the low frequency field, the real part of complex impedance has a strong frequency dependent behaviour, which correlates to higher resistivity and high grain boundary resistance values.

AKNOWLEDGEMENT:

The authors are grateful for the facilities provided by the Department of Physics at Baba Mastnath University, Asthal Bohar, Rohtak.

REFERENCES:

1. T. Sahoo et al., Synthesis and characterization of porous ZnO nanoparticles by hydrothermal treatment of as pure aqueous precursor, Materials Research Bulletin 46.4 (2011): 525-530.
2. S. B. Rana, et al., Synthesis and characterization of pure and doped ZnO nanoparticles, Journal of Optoelectronics and Advanced Materials 12.2 (2010): 257.
3. D. Gao, et al., Room temperature ferromagnetism of pure ZnO nanoparticles, Journal of applied physics 105.11 (2009): 113928.
4. Divya R. "Effect of Azadirachta Indica in Metal Oxide Nanoparticles". International Research Journal on Advanced Science Hub, 2, 8, 2020, 105-111. doi: 10.47392/irjash.2020.102
5. Meinathan S.; Mr. Kannakumar; Gnanavel P. "Experimental investigation on mechanical and FTIR analysis of novel bio materials reinforced epoxy composites". International Research Journal on Advanced Science Hub, 3, Special Issue ICIES-2021 4S, 1970, 58-64.
6. Rashmi S.K; H.S. Bhojya Naik; Jayadevappa H. "Optical and photocatalytic application of ZnFe2O4–SmFeO3 nanocomposites". International Research Journal on Advanced Science Hub, 2, 8, 2020, 123-130. doi: 10.47392/irjash.2020.105
7. Jakeer Husain; Rehana Anjum; Shivaraj G; Gavisiddayya Mathad; Deepa Pathar; Jaisheel Sagar; Bushara Anjum. "Electrical properties of polyaniline/Cadmium Oxide/ZnO Nanocomposites Thin Films". International Research Journal on Advanced Science Hub, 2, 8, 2020, 31-33. doi: 10.47392/irjash.2020.89
8. Jakeer Husain; Rehana Anjum; Narsappa Reddy; Jaisheel Sagar; Bushara Anjum. "AC Conductivity Studies on Polyaniline/Cobalt Oxide Nanocomposites Thin Films". International Research Journal on Advanced Science Hub, 2, 7, 2020, 41-43. doi: 10.47392/irjash.2020.62
9. Gajendiran R; K.Thirumalai raja. "Self-Healing of Wastewater Concrete Using Bacteria". International Research Journal on Advanced Science Hub, 2, 7, 2020, 82-89. doi: 10.47392/irjash.2020.69
10. B. Sharma et al., Synthesis and characterization of polyaniline–ZnO composite and its dielectric behavior, Synthetic metals 159.5-6 (2009): 391-395.
11. P. I. Devi and K. Ramachandran, Dielectric studies on hybridised PVDF–ZnO nanocomposites, Journal of Experimental Nanoscience 6.3 (2011): 281-293.
12. R. Zamiri et al., Structural and dielectric properties of Al-doped ZnO nanostructures, Ceramics International 40.4 (2014): 6031-6036.
13. H. Yadav et al., Eu-doped ZnO nanoparticles for dielectric, ferroelectric and piezoelectric applications, Journal of Alloys and Compounds 689 (2016): 333-341.
14. S. Sagadevan et al., Structural, dielectric and optical investigation of chemically synthesized Ag-doped ZnO nanoparticles composites, Journal of Sol-Gel Science and Technology 83.2 (2017): 394-404.
15. S. Goel et al., 2D porous nanosheets of Y-doped ZnO for dielectric and ferroelectric applications, Journal of Materials Science: Materials in Electronics 29.16 (2018): 13818-13832.